Study the molecular nature of σ, $f_0(980)$, and $a_0(980)$ states

Hiwa A. Ahmed[1,2] and C. W. Xiao[1,*]

[1]*School of Physics and Electronics, Central South University, Changsha 410083, China*
[2]*Physics Department, College of Science, University of Sulaimani, Kurdistan Region 46001, Iraq*

(Received 7 February 2020; accepted 5 May 2020; published 28 May 2020)

We investigate the characteristics of σ, $f_0(980)$, and $a_0(980)$ with the formalism of chiral unitary approach. With the dynamical generation of them, we make a further study of their properties by evaluating the couplings, the compositeness, the wave functions, and the radii. We also research their properties in the single channel interactions, where the $a_0(980)$ cannot be reproduced in the $K\bar{K}$ interactions alone with isospin $I = 1$ since the potential is too weak. In our results, the states of σ and $f_0(980)$ can be dynamically reproduced stably with varying cutoffs both in the coupled channel and the single channel cases. We find that the $\pi\eta$ components is much important in the coupled channel interactions to dynamically reproduce the $a_0(980)$ state, which means that $a_0(980)$ state cannot be a pure $K\bar{K}$ molecular state. We obtain their radii as: $|\sqrt{\langle r^2\rangle}|_{f_0(980)} = 1.80 \pm 0.35$ fm, $|\sqrt{\langle r^2\rangle}|_{\sigma} = 0.68 \pm 0.05$ fm and $|\sqrt{\langle r^2\rangle}|_{a_0(980)} = 0.94 \pm 0.09$ fm. Based on our investigation results, we conclude that the $f_0(980)$ state is mainly a $K\bar{K}$ bound state, the σ state a resonance of $\pi\pi$ and the $a_0(980)$ state a loose $K\bar{K}$ bound state with the significant compositeness of $\pi\eta$. From the results of the compositeness, they are not pure molecular states and have something nonmolecular components, especially for the σ state.

DOI: 10.1103/PhysRevD.101.094034

I. INTRODUCTION

Even though quantum chromodynamics (QCD) is the fundamental theory of strong interaction and governs the high energy region, the nature and the structure of the lowest scalar mesons still problematic and under debate. One of the main topics of the high energy physics is to comprehend the properties of the hadronic resonances. The conventional picture of the hadrons based on the quark model is the baryon made of qqq and the meson $q\bar{q}$. However, that is not the whole picture of the observed hadrons, with the development of the experiments, many resonances have been found, which may have complex structures since their nature cannot be interpreted by the conventional ways, such as tetraquarks [1], hybrids [2], and glueballs [3] for mesons, and pentaquarks and heptaquarks for baryons, or molecular states. These exotic states have drawn much attention both in theories and experiments to understand their structure and decay properties, see more details in the reviews [4–14]. In the low energy region the perturbative QCD failed because of the confinement, so we need to explore a nonperturbative QCD, such as Lattice QCD [15–17], QCD sum rules [18–24], effective field theory [25–27], chiral unitary approach (ChUA) [28–32], and so on. In case of meson-meson and meson-baryon interaction, chiral dynamics is crucial in understanding the structure and the nature of the resonances, and it has shown that many known resonances are dynamically generated in the hadron-hadron interaction [33].

Following the work of Ref. [34], we continue to study the properties of the σ [or $f_0(500)$], $f_0(980)$ [35], and $a_0(980)$ [36] states. Although the states of $f_0(980)$ and $a_0(980)$ are nearly degenerated, they have different isospin and other properties. Several proposals were made about the nature of these scalar particles, such as $q\bar{q}$ state [37–40], multiquark states [1,22–24,41,42], or $K\bar{K}$ molecules [43–46]. The evidence of four-quark nature for the $f_0(980)$ and $a_0(980)$ states are found in the ϕ meson radiative decay [42] where more experimental information and discussions can be referred to Refs. [47–49]. The nature of the σ resonance is different from the other two. The masses of the $f_0(980)$ and $a_0(980)$ are close to the $K\bar{K}$ threshold, conversely σ is far above $\pi\pi$ threshold. Moreover the decay width of the σ is very large, which does not behave like an ordinary Breit-Wigner resonance [50]. Furthermore, from the large N_C limit calculations [51,52] and Regge theory [53] are confirmed that σ is not an ordinary $q\bar{q}$ structure. References [54,55] have found that the states of σ and $a_0(980)$ display a very different N_C behavior. In the work of Ref. [56], using the ChUA, the potential of the pseudoscalars calculated from the chiral Lagrangians [57–

*xiaochw@csu.edu.cn

Published by the American Physical Society under the terms of the Creative Commons Attribution 4.0 International license. Further distribution of this work must maintain attribution to the author(s) and the published article's title, journal citation, and DOI. Funded by SCOAP[3].

62], and then by applying the unitarity in coupled channel scattering amplitudes, the σ, $f_0(980)$ and $a_0(980)$ are dynamically generated. Along the line of Ref. [56], we make a further investigation of the properties of the σ, $f_0(980)$, and $a_0(980)$ states by evaluating their compositeness, the wave functions and the radii both in the coupled channel and the single channel interactions.

In the present work, we will firstly introduce the formalism of the interactions of $K\bar{K}$ and its coupled channels. Then, we discuss the definition of the couplings and how to calculate the compositeness, the wave functions and the radii for a resonance in ChUA. Following, we show our results in details for the cases of the coupled channel and the single channel, respectively. Finally, we close with our conclusions.

II. FORMALISM

In this section, we firstly revisit the formalism of Ref. [56], where the interaction potentials for the coupled channels are derived from the lowest order chiral Lagrangian, and then performing the S-wave projection, the scattering amplitudes are evaluate with a set of on-shell Bethe-Salpeter equations. Next, we introduce the definitions of the couplings in the coupled channel, the wave functions, the compositeness and the radii of the generated resonances.

A. S-wave scattering amplitude in the coupled channels and single channel

In chiral pertubative theory, the most general chiral Lagrangian can be written in a perturbative manner according to the powers of the momenta of the pseudoscalar mesons [57–62],

$$\mathcal{L}_{\rm ChPT}(U) = \sum_n \mathcal{L}_{2n} = \mathcal{L}_2 + \mathcal{L}_4 + \mathcal{O}(p^6), \tag{1}$$

where the lowest order chiral Lagrangian $\mathcal{L}_2$ of the pseudoscalar meson octet is given by

$$\begin{aligned}\mathcal{L}_2 &= \frac{f^2}{4}\langle \partial_\mu U^\dagger \partial^\mu U\rangle + \frac{f^2}{4}\langle M(U^\dagger + U)\rangle \\ &= \frac{1}{2}\langle \partial_\mu \Phi \partial^\mu \Phi\rangle - \frac{1}{2}\langle M\Phi^2\rangle + \frac{1}{12f^2}\langle(\partial_\mu\Phi\Phi - \Phi\partial_\mu\Phi)^2\rangle \\ &\quad + \frac{1}{12f^2}\langle M\Phi^4\rangle + \mathcal{O}\left(\frac{\Phi^6}{f^4}\right),\end{aligned} \tag{2}$$

which has combined with the mass term and contains the kinetic terms (the first two terms) and the interaction terms containing at least four meson fields [59,62]. In the ChUA, we only consider the interaction parts of the lowest order of chiral Lagrangian, the third and the fourth terms, which contain four meson fields. Thus, taking the interaction parts with four meson fields in Eq. (2), the interaction Lagrangian for the ChUA is given by [56],

$$\mathcal{L}_{\rm in} = \frac{1}{12f^2}\langle(\partial_\mu\Phi\Phi - \Phi\partial_\mu\Phi)^2 + M\Phi^4\rangle, \tag{3}$$

where f is the pion decay constant, the value of which is taken as 92.4 MeV [63], $\langle\rangle$ stands for the trace of matrices, and Φ is the pseudo Goldstone boson fields, defined as

$$\begin{aligned}\Phi(x) &= \frac{1}{\sqrt{2}}\phi^a\lambda^a \\ &= \begin{pmatrix} \frac{1}{\sqrt{2}}\pi^0 + \frac{1}{\sqrt{6}}\eta_8 & \pi^+ & K^+ \\ \pi^- & \pi^0 + \frac{1}{\sqrt{6}}\eta_8 & K^0 \\ K^- & \bar{K}^0 & -\frac{2}{\sqrt{6}}\eta_8 \end{pmatrix}.\end{aligned} \tag{4}$$

Besides, the pseudoscalar meson mass matrix M is given by

$$M = \begin{pmatrix} m_\pi^2 & 0 & 0 \\ 0 & m_\pi^2 & 0 \\ 0 & 0 & 2m_K^2 - m_\pi^2 \end{pmatrix}, \tag{5}$$

where we have taken the isospin limit ($m_u = m_d$).

Using the interaction Lagrangian, Eq. (3), we can derive the tree level amplitudes for $K\bar{K}$, $\pi\pi$ and $\pi\eta$ channels, which will be used as the interaction potentials in the coupled channel Bethe-Salpeter equations. After performing the S-wave projections, the interaction potentials in the isospin bases are given by [56],

$$\begin{aligned}V_{11}^{I=0} &= -\frac{1}{4f^2}(3s + 4m_K^2 - \Sigma_i p_i^2), \\ V_{21}^{I=0} &= -\frac{1}{3\sqrt{12}f^2}\left(\frac{9}{2}s + 3m_K^2 + 3m_\pi^2 - \frac{3}{2}\sum_i p_i^2\right), \\ V_{22}^{I=0} &= -\frac{1}{9f^2}\left(9s + \frac{15m_\pi^2}{2} - 3\sum_i p_i^2\right),\end{aligned} \tag{6}$$

$$\begin{aligned}V_{11}^{I=1} &= -\frac{1}{12f^2}\left(3s - \sum_i p_i^2 + 4m_K^2\right), \\ V_{21}^{I=1} &= \frac{\sqrt{3/2}}{12f^2}\left(6s - 2\sum_i p_i^2 + \frac{4}{3}m_\pi^2 - \frac{4}{3}m_K^2\right), \\ V_{22}^{I=1} &= -\frac{1}{3f^2}m_\pi^2,\end{aligned} \tag{7}$$

where we specify the $K\bar{K}$ and $\pi\pi$ channels with the labels 1 and 2, respectively, for the case of isospin $I = 0$, and the $K\bar{K}$ and $\pi\eta$ channels for the case of $I = 1$. For the on shell amplitudes, one can take $p_i^2 = m_i^2$.

For the scattering amplitudes of the coupled channels, one can solve the Bethe-Salpeter equations factorized on shell [56],

$$T = [1 - VG]^{-1}V. \tag{8}$$

It is worthwhile to note that in the present case T, V, and G are 2×2 matrices. The element of the diagonal G matrix is the loop function of two intermediate mesons in the ith channel, given by

$$G_{ii}(s) = i\int \frac{d^4q}{(2\pi)^4}\frac{1}{q^2-m_1^2+i\varepsilon}\frac{1}{(p_1+p_2-q)^2-m_2^2+i\varepsilon}, \tag{9}$$

where p_1 and p_2 are the four-momenta of the two initial particles, respectively, and m_1, m_2 are the masses of the two intermediate particles appearing in the loop. Note that the G function is logarithmically divergent. There are two methods to solve this singular integral, either using the three-momentum cutoff method [56], where the analytic expression is given by Ref. [64], or the dimensional regularization method [65]. Using the cutoff method we can rewrite Eq. (9) as

$$G_{ii}(s) = \int_0^{q_{\max}} \frac{q^2dq}{(2\pi)^2}\frac{\omega_1+\omega_2}{\omega_1\omega_2[s-(\omega_1+\omega_2)^2+i\epsilon]}, \tag{10}$$

where $q=|\vec{q}|$, $\omega_i=(\vec{q}^2+m_i^2)^{1/2}$ and $s=(p_1+p_2)^2$, and the cutoff, $q_{\max}$, is the only one free parameter. We show our results of the real part and the imaginary part of the G functions in the isospin $I=0$ case in Fig. 1 with two different cutoffs (about their values see the discussions at the beginning of next section), where one can see that the imaginary part of the loop function is independent with the cutoff, which leads to extrapolate to the second Riemann sheet easily, see the discussions below.

Using ChUA, one also can easily determine the masses and the decay widths of the states produced in the coupled channel interactions just by looking for the poles in the complex Riemann sheets. Thus, one need to extrapolate the analytical structure of the scattering amplitudes in the complex s plane. To fulfill these, one can extrapolate the $G(s)$ function into the second Riemann sheet by

$$\begin{aligned} G_{ii}^{(II)}(s) &= G_{ii}^{(I)}(s) - 2i\mathrm{Im}G_{ii}^{(I)}(s) \\ &= G_{ii}^{(I)}(s) + \frac{i}{4\pi}\frac{p_{cmi}(s)}{\sqrt{s}}, \end{aligned} \tag{11}$$

where the loop function on the first Riemann sheet, $G_{ii}^{(I)}(s)$, is given by Eq. (10), and the three momentum in center-of-mass (CM) frame is given by

$$p_{cmi}(s) = \frac{\lambda^{1/2}(s,m_1^2,m_2^2)}{2\sqrt{s}}, \tag{12}$$

with the usual Källen triangle function $\lambda(a,b,c) = a^2+b^2+c^2-2(ab+ac+bc)$, see more details in

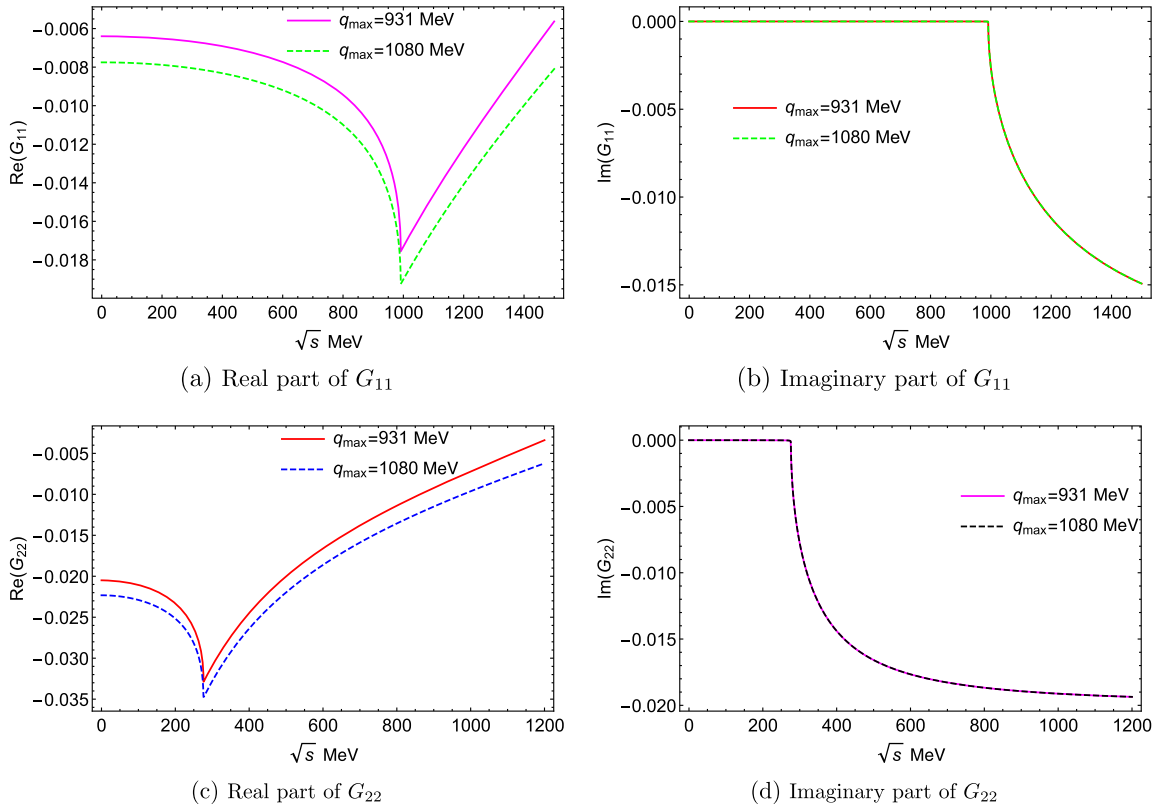

(a) Real part of G_{11} (b) Imaginary part of G_{11}

(c) Real part of G_{22} (d) Imaginary part of G_{22}

FIG. 1. Real part and imaginary part of the propagator for the case of isospin $I=0$ with two different cutoffs $q_{\max}$.

Ref. [56]. In our case of two coupled channels, there are four Riemann sheets, defined as

Sheet I: $\mathrm{Im}p_1 > 0, \mathrm{Im}p_2 > 0 \to G_{11}^{(I)}, G_{22}^{(I)}$;
Sheet II: $\mathrm{Im}p_1 > 0, \mathrm{Im}p_2 < 0 \to G_{22}^{(II)}, G_{11}^{(I)}$;
Sheet III: $\mathrm{Im}p_1 < 0, \mathrm{Im}p_2 < 0 \to G_{22}^{(II)}, G_{11}^{(II)}$;
Sheet IV: $\mathrm{Im}p_1 < 0, \mathrm{Im}p_2 > 0 \to G_{22}^{(I)}, G_{11}^{(II)}$.

In the present case, only two coupled channels, the elements of the scattering amplitudes T matrix can be written as [56],

$$T_{11} = \frac{1}{\Delta_c}(\Delta_\pi V_{11} + V_{12}^2 G_{22}),$$
$$T_{21} = \frac{1}{\Delta_c}(V_{21} G_{11} V_{11} + \Delta_k V_{21}),$$
$$T_{22} = \frac{V_{22}}{\Delta\pi} + \frac{V_{12}^2 G_{11}}{\Delta_\pi \Delta_c}, \tag{13}$$

where one defines

$$\Delta_\pi = 1 - V_{22} G_{22},$$
$$\Delta_K = 1 - V_{11} G_{11},$$
$$\Delta_c = \Delta_K \Delta_\pi - V_{12}^2 G_{11} G_{22}. \tag{14}$$

For the single channel cases, we have the $K\bar{K}$ and $\pi\pi$ ($\pi\eta$) interaction channel separately for $I = 0$ ($I = 1$). Just by taking $V_{21} = 0$, one can easily reduce Eq. (13) to,

$$T_{11} = \frac{V_{11}}{\Delta_k}, \qquad T_{22} = \frac{V_{22}}{\Delta\pi}. \tag{15}$$

B. The couplings and the wave functions

By applying the Laurent expansion of the amplitude close to the pole, the scattering amplitudes can be written as [66,67]

$$T_{ij} = \frac{g_i g_j}{s - s_{\mathrm{pole}}} + \gamma_0 + \gamma_1 (s - s_{\mathrm{pole}}) + \cdots, \tag{16}$$

where g_i and g_j are the coupling constants of the ith and jth channels, which can be calculated from the residue of the pole [68,69]

$$g_i g_j = \lim_{s \to s_{\mathrm{pole}}} (s - s_{\mathrm{pole}}) T_{ij}. \tag{17}$$

Using Cauchy integral formula, we can evaluate the residue as a loop integral in the complex s plane,

$$g_i^2 = \frac{1}{2\pi i} \oint T_{ii} ds, \tag{18}$$

where the integral is over a closed path in the complex s plane around the pole $s = s_{\mathrm{pole}}$. Furthermore, with the couplings of the corresponding poles, one can generalize Weinberg's rule [70] for bound state or resonance to the formalism of ChUA [71]

$$-\sum_i g_i^2 \left[\frac{dG_i}{ds}\right]_{s=s_{\mathrm{pole}}} = 1, \tag{19}$$

where an alternative derivation of this relationship can be found in Ref. [72]. The sum rule of Eq. (19) holds for the pure molecular states, the bound states or resonances, which are dynamically generated in the coupled channel interactions. More discussions and the applications of this rule can be found in Refs. [73–77]. However, in some cases, if a physical state couples not only to hadron-hadron pairs, but also to a different component of nonmolecular type, this relation becomes for the composite states

$$-\sum_i g_i^2 \left[\frac{dG_i}{ds}\right]_{s=s_{\mathrm{pole}}} = 1 - Z, \tag{20}$$

where Z represents the probability of which the system is not a molecule components but something else. As discussed in Ref. [76], the interpretation of Z as a probability nonmolecular (meson-meson or meson-baryon state in ChUA) component is strict for bound states, which is related to the genuine component in the wave function of the state omitted from the coupled channels. Note that for a specified channel the G_i function should be extrapolated to the right Riemann sheet for a corresponding pole of the state.

To understand more about the sources of the resonances, we study the wave function of the resonance at small distances. Once we have the wave function of a resonance, one can also investigate its form factor, which responses the state to external sources. Following the formalism of Ref. [78], the wave function of a resonance in coordinate space is given by

$$\phi(\vec{r}) = \int_{q_{\max}} \frac{d^3\vec{p}}{(2\pi)^{3/2}} e^{i\vec{p}\cdot\vec{r}} \langle \vec{p} | \Psi \rangle. \tag{21}$$

After performing the angle integration of the momentum, we obtained [68]

$$\phi(\vec{r}) = \frac{1}{(2\pi)^{3/2}} \frac{4\pi}{r} \frac{1}{C} \int_{q_{\max}} p dp \sin(pr) \times \frac{\Theta(q_{\max} - |\vec{p}|)}{E - \omega_1(\vec{p}) - \omega_2(\vec{p})} \frac{m_V^2}{\vec{p}^2 + m_V^2}, \tag{22}$$

where C is the normalization constant, and $E \equiv \sqrt{s_{\mathrm{pole}}}$, thus, which is real for a pure bound state with zero width and otherwise complex for the general cases in ChUA. Note that here we put an extra form factor $f(\vec{q}) = \frac{m_V^2}{\vec{p}^2 + m_V^2}$ to

regulate the scale of the wave function, and our conclusions do not change if we remove it. Besides, Eq. (22) is the scattering wave function of the two components, which does not include the outgoing plane wave function for the case of the resonance with open channel(s), and thus, it will be confined within a few fm for the molecular states,[1] see our results later. Using the wave functions that we have, one can evaluate the form factor of the states with its definition [78],

$$F(\vec{q}) = \int d^3\vec{r}\phi(\vec{r})\phi^*(\vec{r})e^{-i\vec{q}\cdot\vec{r}} = \int d^3\vec{p} \times \frac{\theta(\Lambda-p)\theta(\Lambda-|\vec{p}-\vec{q}|)}{[E-\omega_1(p)-\omega_2(p)][E-\omega_1(\vec{p}-\vec{q})-\omega_2(\vec{p}-\vec{q})]}, \tag{23}$$

with a normalization to keep $F(q=0)\equiv 1$. For a generated state in ChUA, a pole with its width, which is complex, the form factor is complex too, see the results below. Finally, the radii of the states (or mean square distance) can be evaluated from the form factor,

$$\langle r^2\rangle = -6\left[\frac{\mathrm{d}F(q)}{\mathrm{d}q^2}\right]_{q^2=0}. \tag{24}$$

Note that a soft step function needed to make the form factor converge in this case. On the other hand, for the case of a bound state, the radii of the state can also be obtained from the tail of the wave functions as done in Ref. [73]

$$\langle r^2\rangle_i = \frac{-g_i^2\left[\frac{\mathrm{d}G_i(s)}{\mathrm{d}s}\right]_{s=s_{\rm pole}}}{4\mu_i B_{\mathrm{E},i}}, \tag{25}$$

where the binding energy $B_{\mathrm{E},i} = m_i + m_i' - M_{\mathrm{B}}$, and the reduced mass $\mu_i = \frac{m_i m_i'}{m_i+m_i'}$. Conceptually, $\langle r^2\rangle_i$ is the mean-squared distance of the bound state in the ith channel. In fact, using the relations of the sum rule and the wave functions, it is easy to know that Eq. (25) is an approximation of Eq. (24), see more discussions in Refs. [71,72,76,84].

III. RESULTS

We first revisit the $K\bar{K}$ interactions with its coupled channels of $\pi\pi$ or $\pi\eta$, where the states of σ, $f_0(980)$, and $a_0(980)$ are dynamically generated in the coupled channel interactions as done in Ref. [56]. But, we make a further study of the couplings, the compositeness, the wave functions and the radii for these states to investigate more details on their properties, as the results shown below. To find more information about the structure of the poles corresponding to these states, we examine the single channel interactions. Note that, for the only one free parameter in our approach, what we used below for the value of the cutoff is the one determined in Ref. [34] by performing a combined fit for the experimental data, $q_{\rm max} = 931$ MeV, which is a bit different with the ones used in Ref. [56]. To see the uncertainties of our calculations, we also show the results with the one of about 15% division to the upper limits, $q_{\rm max} = 1080$ MeV and varying the values between 15% division in some cases.

A. Coupled channel approach

We first calculate the phase shifts and the inelasticities. As done in Ref. [56], the two-channels S-matrix are used,

$$S = \begin{bmatrix} \eta e^{2i\delta_1} & i(1-\eta^2)^{1/2}e^{i(\delta_1+\delta_2)} \\ i(1-\eta^2)^{1/2}e^{i(\delta_1+\delta_2)} & \eta e^{2i\delta_2} \end{bmatrix} \tag{26}$$

where the observables of δ_1, δ_2 correspond to the phase shifts of the channel 1, 2, respectively, and the one of η is the inelasticity. These observables can be calculated from the relationship between S-matrix and the scattering amplitude T-matrix, having

$$T_{11} = -\frac{8\pi\sqrt{s}}{2ip_{cm1}}(S_{11}-1),$$
$$T_{22} = -\frac{8\pi\sqrt{s}}{2ip_{cm2}}(S_{22}-1),$$
$$T_{12} = t_{21} = -\frac{8\pi\sqrt{s}}{2i\sqrt{p_{cm1}p_{cm2}}}(S_{12}-1), \tag{27}$$

where p_{cmi} is the corresponding three momentum in the CM frame as discussed above. The results of the phase shifts and the inelasticities in isospin of $I=0$ and $I=1$ sectors are shown in Figs. 2 and 3, respectively. In Fig. 2, we can see that the results of $I=0$ sector are in good agreement with the experimental data up to $\sqrt{s}=1.2$ GeV even with the upper limit of the cutoff. From Fig. 2(b), one can see that the σ structure is a wide bump and the signal of $f_0(980)$ is in the sharp increasing region which crosses 90° [50]. However, in $I=1$ sector because of the lack of experimental data for phase shifts and inelasticities, we make some predictions for them, where the structure of $a_0(980)$ can be clearly seen in the phase shifts of the $\pi\eta$ channel.

Next, we show our results for the invariant mass distributions. As done in Ref. [56], we compare our results

[1]Within ChUA, more discussions about the wave functions for the s-wave bound states can be found in Ref. [79], for the s-wave resonances with open channel(s) in Refs. [76,78], the extrapolation to any partial wave interactions in Ref. [71], and more details connected with the sum rule in Refs. [71,80]. Furthermore, Refs. [81–83] have discussed more about the wave functions for the molecular state and the compact four-quark states.

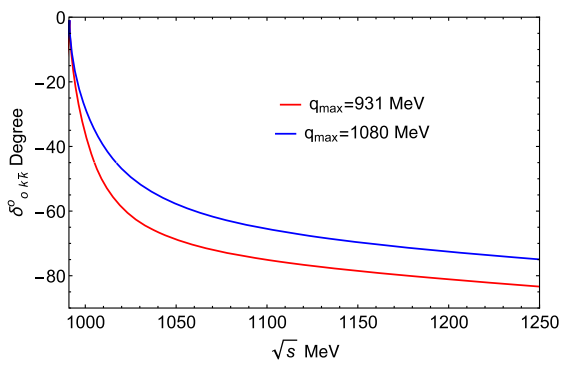

(a) Results of $K\bar{K}$ phase shifts.

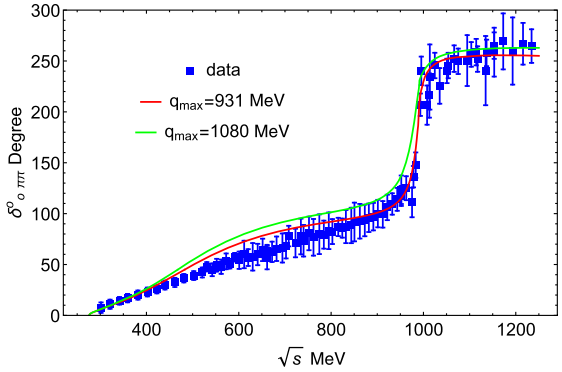

(b) Results of $\pi\pi$ phase shifts.

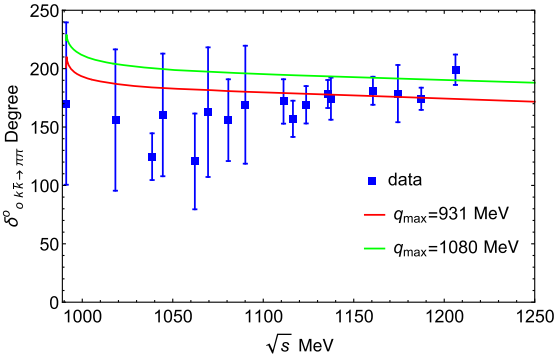

(c) Results of $K\bar{K} \to \pi\pi$ phase shifts.

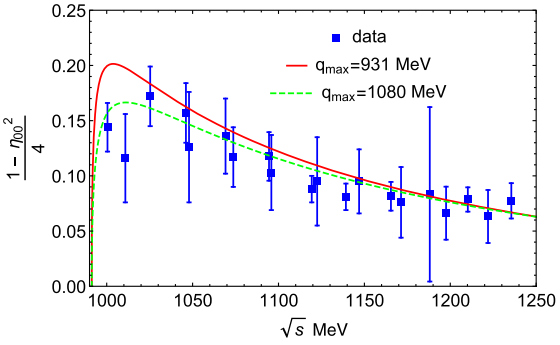

(d) Results of inelasticities $\frac{(1-\eta_{00}^2)}{4}$.

FIG. 2. Our results for the sector of isospion $I = 0$ with two different values of $q_{\max}$.

with the data of $\pi\eta$ invariant mass distribution from the reaction $K^- p \to \Sigma(1385)\pi^-\eta$ and the ones of $K\bar{K}$ from the reaction $K^- p \to \Sigma^+ K^- K^0$, see Fig. 4, where we use

$$\frac{d\sigma_{ii}}{d\sqrt{s}} = C|T_{ii}|^2 q_{cmi}, \tag{28}$$

where T_{ii} is the scattering amplitude of the $K\bar{K}$ or $\pi\eta$ channel, q_{cmi} is three momentum in CM frame and C the normalization factor. To see more clearly the resonances dynamically reproduced in the coupled channel interactions, we plot the modulus squared of the scattering amplitudes in $I = 0$ and $I = 1$ sectors, as shown in Figs. 5 and 6. From Figs. 5(a) and 5(b) of $|T_{11}|^2$ and $|T_{12}|^2$ for $I = 0$, the peak of $f_0(980)$ state is clearly seen. In Fig. 5(c), the broad structure of T_{22} are σ resonance, where the dip is the signal of $f_0(980)$ state closed to the $K\bar{K}$ threshold and the structure of the amplitudes are consistent with the ones calculated with dispersion method [85]. Likewise, the $a_0(980)$ resonance can be clearly seen in $|T_{11}|^2$, $|T_{12}|^2$, and $|T_{22}|^2$ for $I = 1$ sectors in Fig. 6. In spite of showing the $a_0(980)$ resonance in the results of $|T_{22}|^2$, see Fig. 6(c), there is an extra feature, which is called threshold effect [56,86], of which more details can be seen a recent review [87]. This feature is due to the strong coupling of the resonance $a_0(980)$ to the $K\bar{K}$ channel which cause to dwindle the width of the scattering amplitude and change the location of the maximum. This effect is originated from the second term of T_{22}, $\frac{V_{12}^2 G_{11}}{\Delta_\pi \Delta_c}$, see Eq. (13), and precisely comes from the imaginary part of the term $\frac{G_{11}}{\Delta_c}$ as shown in Fig. 7.

In Figs. 5 and 6, we have dynamically reproduced the states of σ, $f_0(980)$ and $a_0(980)$ in the modulus squared of the scattering amplitudes. Thus, we can search for their corresponding poles in the Riemann sheets to determine their masses and widths. To see their poles stable or not, we plot the trajectories for the masses and the widths of their poles by changing the value of $q_{\max}$, see Fig. 8, where all of these poles are found in the second Riemann sheet (sheet II as defined in the last section). Because all of these poles locate in the second Riemann sheet, where the channel of $\pi\pi$ or $\pi\eta$ is open and $K\bar{K}$ close, we only can obtain rough information on their structures since all of them are above the threshold of $\pi\pi$ or $\pi\eta$ channel and below the one of $K\bar{K}$. This is why we need to continue researching their couplings of a certain channel later for revealing more structure details. From Fig. 8, we can find that even varying the free parameter, $q_{\max}$, the corresponding poles for them are stably produced in the second Riemann sheets. But, one can see that the behavior of the pole for σ is different from

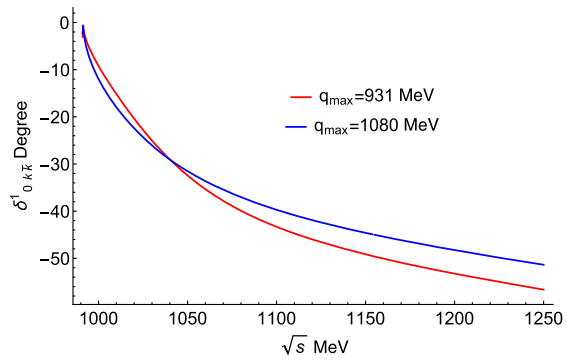

(a) Results of $K\bar{K}$ phase shift.

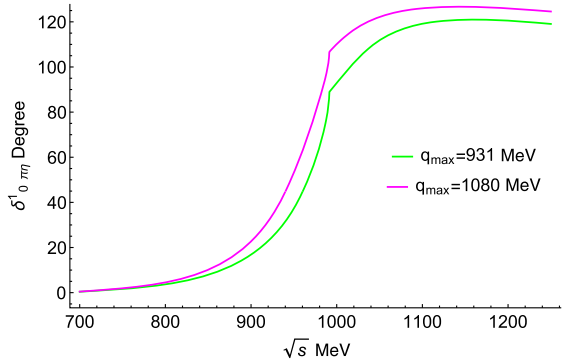

(b) Results of $\pi\eta$ phase shift.

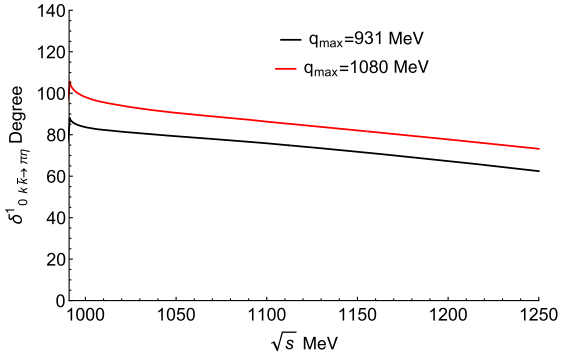

(c) Results of $K\bar{K} \to \pi\eta$ phase shift.

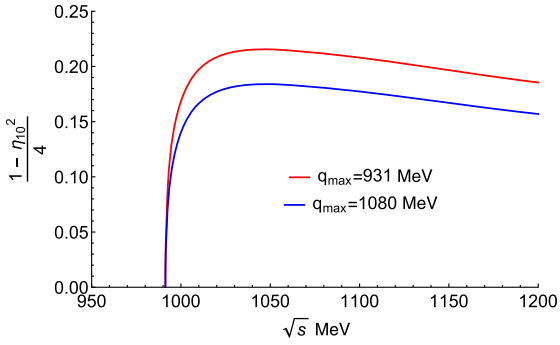

(d) Results of inelasticities $\frac{(1-\eta_{10}^2)}{4}$.

FIG. 3. Our results for the sector of $I = 1$.

the other two states, $f_0(980)$ and $a_0(980)$. When the cutoff increases, the mass of σ slightly increases to a maximum and then declines, and its width decreases, whereas the masses of $f_0(980)$ and $a_0(980)$ always decline from above $K\bar{K}$ threshold to below threshold, and their widths increase (the width of $a_0(980)$ increase to an upper limit). These differences mean that the properties of σ look like different from the ones of $f_0(980)$ and $a_0(980)$. On the other hand, the mass of $f_0(980)$ is more stable than the one of $a_0(980)$, whereas, the width of $a_0(980)$ does not change much when the cutoff varies. Thus, we continue to make further investigations about their different properties.

To explain the different properties of the states σ, $f_0(980)$ and $a_0(980)$ in the behaviors of Fig. 8, we firstly look at the results of G functions in Fig. 1, where one can see that the real parts of the loop function reduce when the cutoff $q_{\max}$ increases, whereas the imaginary parts are independent with the cutoff. To simplify the discussions,

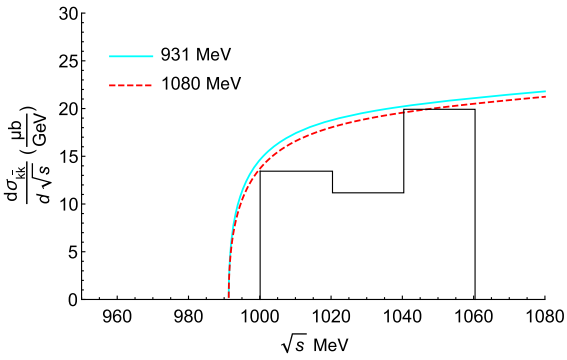

(a) The invariant mass distribution of $K\bar{K}$ ($C = 2.5 \times 10^{-5}$).

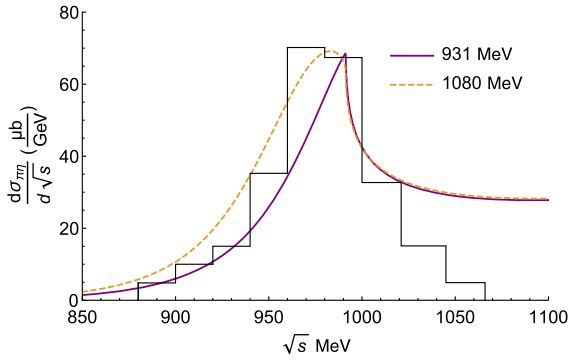

(b) The invariant mass distribution of $\pi\eta$ ($C = 3.63 \times 10^{-5}$).

FIG. 4. Results for the invariant mass distribution with two different $q_{\max}$.

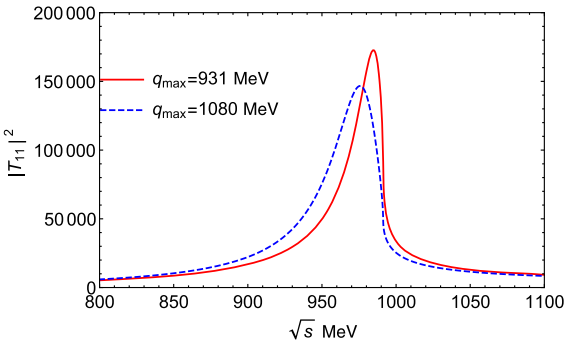

(a) Results of $|T_{11}|^2$ for the $K\bar{K}$ channel.

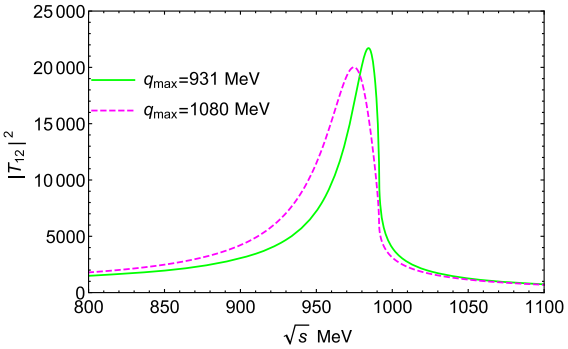

(b) Results of $|T_{12}|^2$ for the $K\bar{K} \to \pi\pi$ channel.

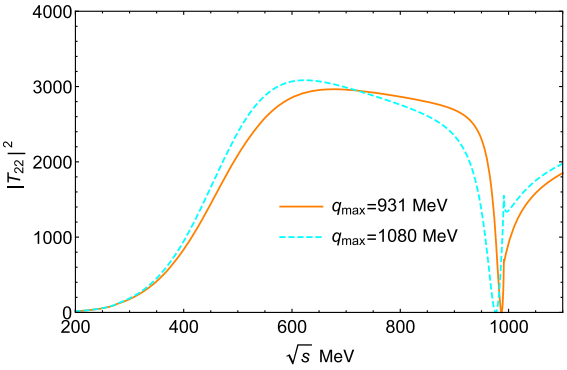

(c) Results of $|T_{22}|^2$ for the $\pi\pi$ channel.

FIG. 5. Results of the modulus squared of the scattering amplitudes in $I = 0$ sector.

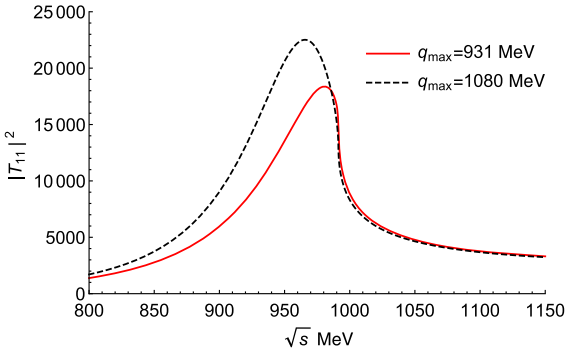

(a) Results of $|T_{11}|^2$ for the $K\bar{K}$ channel.

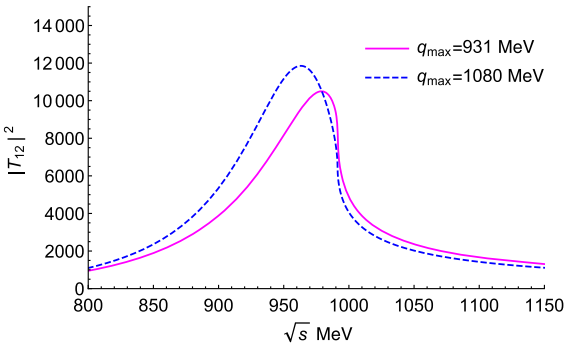

(b) Results of $|T_{12}|^2$ for the $K\bar{K} \to \pi\eta$ channel.

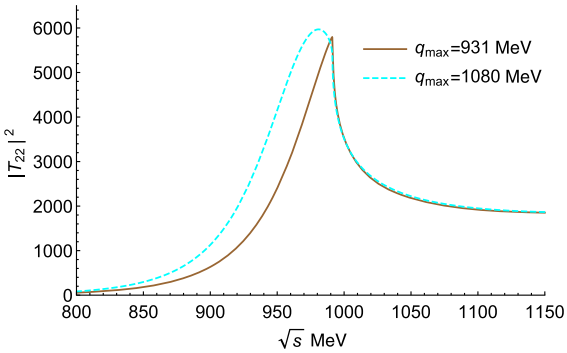

(c) Results of $|T_{22}|^2$ for the $\pi\eta$ channel.

FIG. 6. Results of the modulus squared of the scattering amplitudes in $I = 1$ sector.

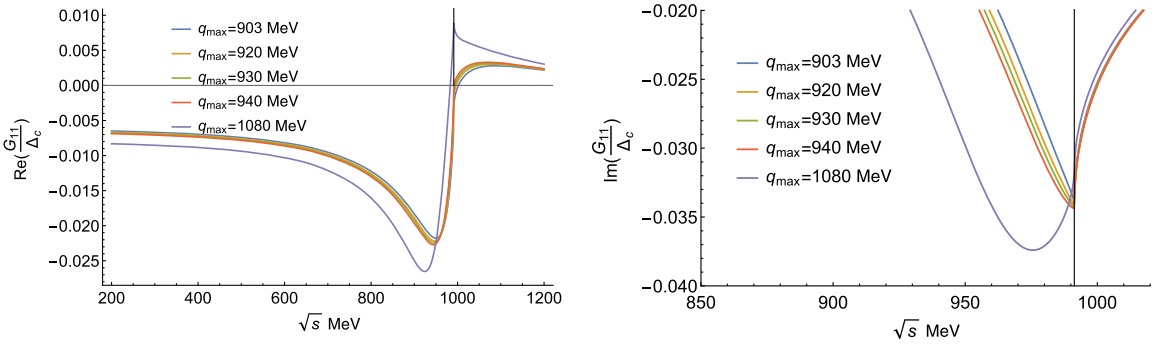

FIG. 7. Results of the real part (left) and imaginary (right) part of $(\frac{G_{11}}{\Delta_c})$ with different cutoffs.

we detail with the single channel formalism, since these properties can be confirmed by the single channel cases, except for the one of $a_0(980)$, see the discussions on the next subsection and the results of Fig. 13. Since the σ state is a resonance above the $\pi\pi$ threshold of which the pole is located in the second Riemann sheet, one can see that the pole conditions are the modulus and the arguments of complex G_{22} and V_{22} meeting with both $|V_{22}G_{22}| = 1$

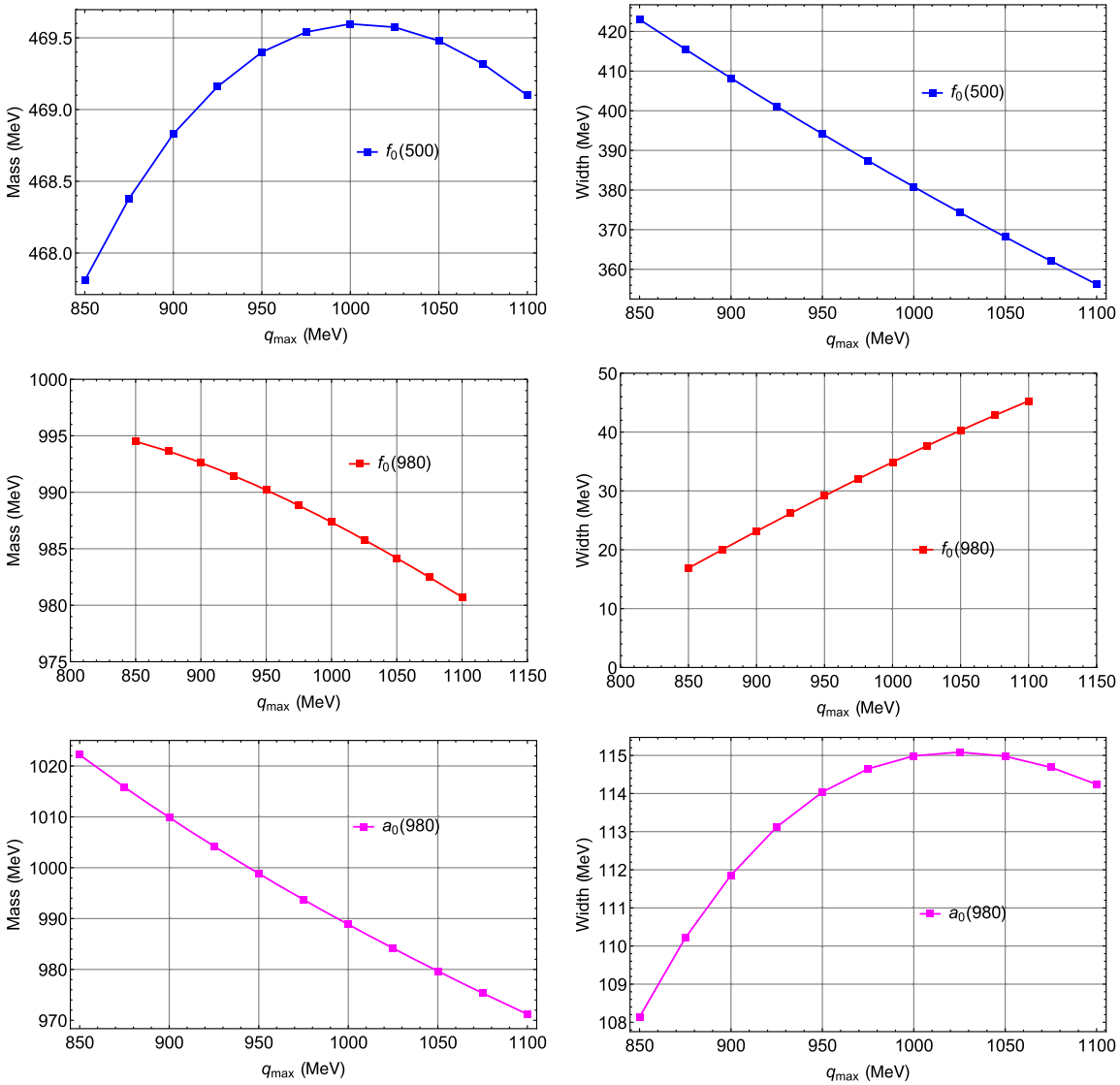

FIG. 8. Trajectories for the masses and the widths of the poles in the second Riemann sheets corresponding to σ ($f_0(500)$), $f_0(980)$, and $a_0(980)$ by varying cutoff ($q_{\max}$).

and $\mathrm{Arg}(V_{22}) = -\mathrm{Arg}(G_{22})$, which are equivalent to $1 - \mathrm{Re}(V_{22}G_{22}) = 0$ and $\mathrm{Im}(V_{22}G_{22}) = 0$, see the subfigures of Fig. 9(a) and Fig. 9(b). From Fig. 9(a), one can find that, when the cutoff $q_{\max}$ increases, the parts of $\frac{1}{|G_{22}|}$ close to x-axes (real energy) will rise up due to the real parts of G function decreasing, which will lead to the pole moving to higher energy, and thus, the mass of the σ state increases, as shown in Fig. 8. On the other hand, one also can see that the surface of $\frac{1}{|G_{22}|}$ is a bit flat, which make the pole moving to higher energy not much. This is why the mass of the σ state increases in a small range. In Fig. 9(b), when the cutoff $q_{\max}$ increases, the arguments of the complex G_{22}, $-\mathrm{Arg}(G_{22})$, increase. But, on the other hand, the real parts of G function decrease, which will lead to the imaginary parts of G function reducing more, and thus, the width of the σ state decreasing more, see Fig. 8. For the case of the state of $f_0(980)$, since it is a bound state of $K\bar{K}$ which is the dominant channel for the $f_0(980)$ state in the coupled channel interactions, it is easy to see in Fig. 9(c) that the mass of the $f_0(980)$ state decreases due to the cutoff increasing, where we plot $\frac{1}{V_{11}}$ and $\mathrm{Re}(G_{11})$ for the $K\bar{K}$ channel. But, the width of the $f_0(980)$ state comes from the contributions of the $\pi\pi$ channel, and thus, from the discussions for the σ state, the width will become larger for the pole moving to the lower energy region with the cutoff increasing. In the case of the state of $a_0(980)$, it looks like a bit complicated for the potential of the $K\bar{K}$ channel being too weak to create a pole in the first Riemann sheet in the single channel case, see the discussions on the next subsection. In fact, one can perform similar analyses with the pole conditions as the case of the σ state replacing with the parts of $\Delta_c - 1$, see Eq. (14), where we do not repeat this analyses again. One should know that in this case the transition potential of V_{12} plays a significant role to produce a pole in the second Riemann sheet of the coupled channel case. Besides, the width of the $a_0(980)$ state is not changed much for the cutoff varying because of the constant potential of the $\pi\eta$ channel, see Eq. (7).

For the sake of the complete investigations about the characteristics of these resonances, we continue to study the couplings, the compositeness, the wave functions and the radii as well. The couplings to various channels for isospin $I = 0$ and $I = 1$ sectors have been calculated using

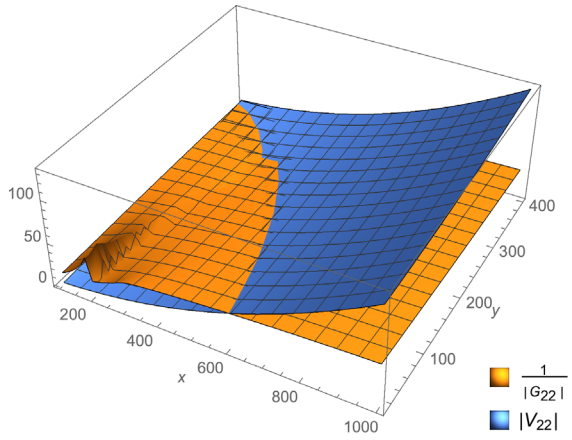

(a) Results of $\frac{1}{|G_{22}|}$ and $|V_{22}|$ in the complex energy planes.

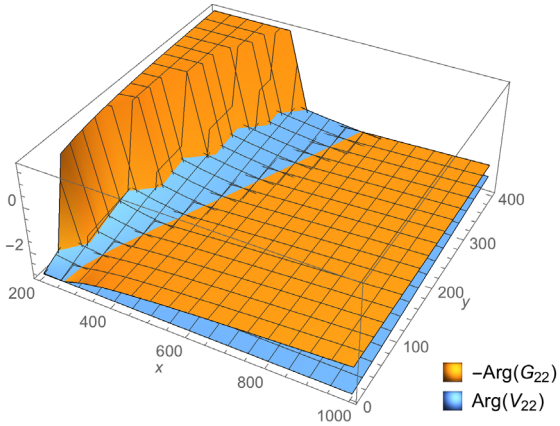

(b) Results for the arguments of the complex G_{22} and V_{22}.

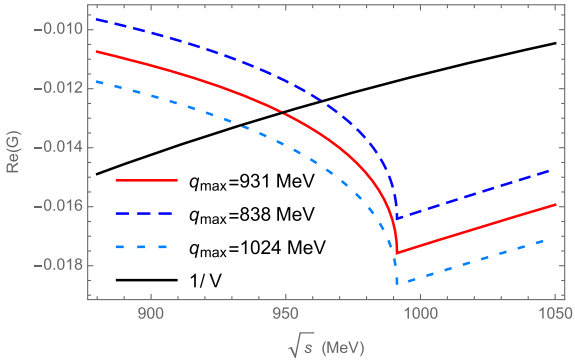

(c) Results of $\frac{1}{|V_{11}|}$ and $|G_{11}|$ with the real energy $\sqrt{s}$.

FIG. 9. Results of the potentials V and the loop functions G ($\sqrt{s} = x + iy$).

Eq. (17), as presented in Tables I and II, respectively. From these results in $I = 0$ sector, it is observed that the σ state couples to the $\pi\pi$ channel strongly, while f_0 strongly couples to the $K\bar{K}$ channel. Thus, the pole of the σ state dominates by the $\pi\pi$ channel whereas the one of the f_0 state mainly by the $K\bar{K}$ channel. In $I = 1$ sector, the a_0 state is tightly coupled to both the $K\bar{K}$ and $\pi\eta$ channels, but it has more tendency to the $K\bar{K}$ channel, which means that the pole of a_0 is dominated by the $K\bar{K}$ channel but the contributions of $\pi\eta$ is significant too.

Using the sum rule of Eq. (20), the compositeness can be calculated from the couplings of the dynamically generated states, where one can check that whether f_0 and a_0 are a pure molecular state or have something else. Our results are given in Tables III and IV. From the results of Table III, once again we can conclude that the structure of f_0 is highly dominated by the $K\bar{K}$ molecular components, which is up to 80% with the central value of $q_{\max} = 931$ MeV, and has very small parts of the $\pi\pi$ components even though the coupling to the $\pi\pi$ channel is not so small, which is more than $1/3$ of the one to the $K\bar{K}$ channel, see Table I. By contrast, the σ state has large part components of $\pi\pi$ about 40% and quite tiny parts of $K\bar{K}$, where one can find that this state still has much large parts of nonmolecular components. Our results of the compositeness in Table III for the states of σ and f_0 are consistent with the ones obtained in Ref. [77] with the inverse amplitude method. The a_0 state has a main components of $K\bar{K}$ and some contributions from the $\pi\eta$ component, see Table IV, but it still has something else about 30%. These results are comparable with the work of Ref. [73] where the properties of these resonances are investigated with the formalism of finite-volume. Therefore, these states are not pure molecular states and have something else, where Ref. [88] also

TABLE I. Couplings of σ and f_0 to every channel for $I = 0$ sector.

$q_{\max} = 931$ MeV	$g_{K\bar{K}}g_{K\bar{K}}(\mathrm{GeV}^2)$	$\lvert g_{K\bar{K}}\rvert(\mathrm{GeV})$	$g_{\pi\pi}g_{\pi\pi}(\mathrm{GeV}^2)$	$\lvert g_{\pi\pi}\rvert(\mathrm{GeV})$
σ: $469.23 + 199.70i$	$-1.05 + 1.72i$	1.42	$-3.49 + 8.20i$	2.98
f_0: $991.17 + 13.45i$	$10.92 - 10.91i$	3.92	$-1.76 + 0.70i$	1.37
$q_{\max} = 1080$ MeV				
σ: $469.28 + 180.46i$	$-0.80 + 1.86i$	1.42	$-2.0 + 8.28i$	2.92
f_0: $982.13 + 21.67i$	$16.15 - 10.55i$	4.39	$-2.34 + 1.11i$	1.60

TABLE II. Couplings of a_0 for $I = 1$ sector.

$q_{\max} = 931$ MeV	$g_{K\bar{K}}g_{K\bar{K}}(\mathrm{GeV}^2)$	$\lvert g_{K\bar{K}}\rvert(\mathrm{GeV})$	$g_{\pi\eta}g_{\pi\eta}(\mathrm{GeV}^2)$	$\lvert g_{\pi\eta}\rvert(\mathrm{GeV})$
a_0: $1002.90 + 56.68i$	$24.17 - 9.22i$	5.08	$10.30 + 5.71i$	3.43
$q_{\max} = 1080$ MeV				
a_0: $974.50 + 57.31i$	$21.83 - 3.28i$	4.78	$8.16 + 5.20i$	3.11

TABLE III. Results of the compositeness of the poles in $I = 0$ sector.

$q_{\max} = 931$ MeV	$(1 - Z)_{K\bar{K}}$	$\lvert(1 - Z)_{K\bar{K}}\rvert$	$(1 - Z)_{\pi\pi}$	$\lvert(1 - Z)_{\pi\pi}\rvert$
σ: $469.23 + 199.70i$	$-0.01 + 0.01i$	0.01	$-0.13 - 0.37i$	0.40
f_0: $991.17 + 13.45i$	$0.79 + 0.12i$	0.80	$0.02 - 0.01i$	0.02
$q_{\max} = 1080$ MeV				
σ: $469.28 + 180.46i$	$-0.00 + 0.01i$	0.01	$-0.16 - 0.36i$	0.39
f_0: $982.13 + 21.67i$	$0.70 + 0.11i$	0.70	$0.02 - 0.01i$	0.02

TABLE IV. Results of the compositeness of the poles in $I = 1$ sector.

$q_{\max} = 931$ MeV	$(1 - Z)_{K\bar{K}}$	$\lvert(1 - Z)_{K\bar{K}}\rvert$	$(1 - Z)_{\pi\eta}$	$\lvert(1 - Z)_{\pi\eta}\rvert$
a_0: $1002.90 + 56.68i$	$0.37 + 0.41i$	0.55	$-0.09 - 0.13i$	0.16
$q_{\max} = 1080$ MeV				
a_0: $974.50 + 57.31i$	$0.34 + 0.29i$	0.45	$-0.07 - 0.12i$	0.14

conclude that the $f_0(980)$ and $a_0(980)$ states are not elementary states based with a Flatté parametrization analysis.

To study the response of these states to the external sources, one need to know the form factor of these states. Thus, we evaluate the wave functions for them, and then, we can calculate the radii once we have their form factor. The wave functions of these state for all distances are shown in Fig. 10, where the real parts and the imaginary parts of the wave functions for the f_0, σ and a_0 states are given since the poles corresponding to these states are complex. From Fig. 10, one can see that, up to about 4 fm, the wave functions for them become zero. With the wave functions obatined, we can investigate the radii of these states with Eq. (24) which relates the wave functions at the origin, see the results of Table V with two cutoffs. As discussed above, we also calculate the radii from the tail of the wave functions using Eq. (25), as shown in Table VI. From the results of Tables V and VI, we can clearly see that the radii of the f_0 and a_0 states in two approaches of Eqs. (24) and (25) are larger than the typical hadronic scale 0.8 fm [73], whereas the one of the σ state keeps in the typical hadronic scale $\lesssim$0.8 fm. But, in Table VI, we find that the one for $f_0(980)$ with cutoff $q_{\max} = 931$ MeV is much larger, $|\sqrt{\langle r^2\rangle}| = 16.36$ fm, which is due to the corresponding pole closing to the $K\bar{K}$ threshold where the binding energy becomes zero, see Eq. (25). Indeed, when we vary the cutoff which changes the positions of the corresponding poles closed to the threshold, the results with Eq. (25) become unstable, as shown in Fig. 11. In Fig. 11,

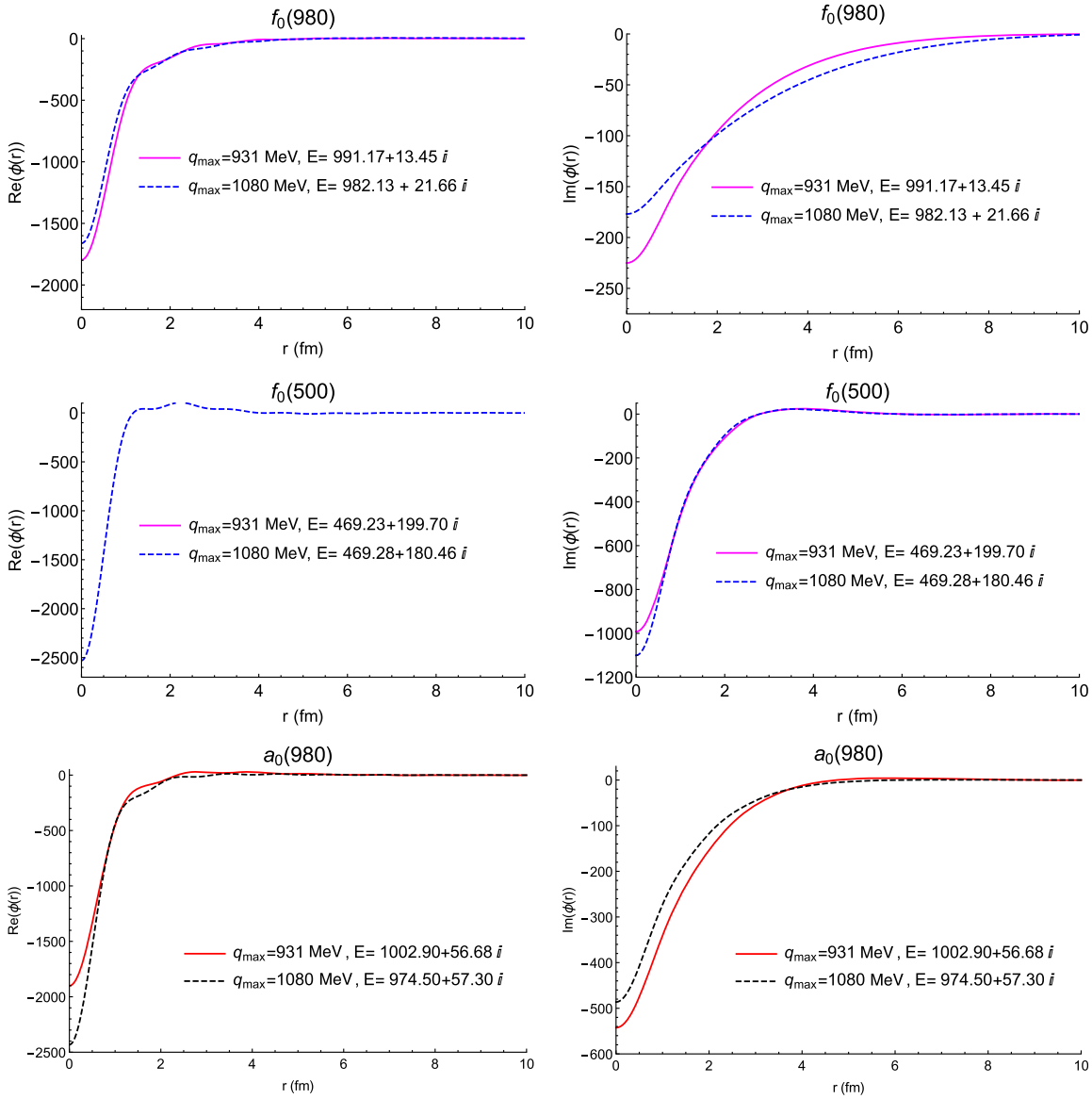

FIG. 10. Results of the real part and imaginary part of the wave functions for the f_0 (upper parts), σ (middle parts), and a_0 (lower parts) states.

TABLE V. The radii of states calculated with Eq. (24).

Resonances	$q_{\max} = 931$ MeV	$\lvert\sqrt{\langle r^2\rangle}\rvert$	$q_{\max} = 1080$ MeV	$\lvert\sqrt{\langle r^2\rangle}\rvert$
f_0	$1.42 + 1.10i$ fm	1.80 fm	$1.31 + 0.62i$ fm	1.45 fm
σ	$0.68 + 0.005i$ fm	0.68 fm	$0.63 + 0.04i$ fm	0.63 fm
a_0	$0.83 + 0.44i$ fm	0.94 fm	$0.96 + 0.35i$ fm	1.03 fm

TABLE VI. The radii of states evaluated with Eq. (25).

Resonances	$q_{\max} = 931$ MeV	$\lvert\sqrt{\langle r^2\rangle}\rvert$	$q_{\max} = 1080$ MeV	$\lvert\sqrt{\langle r^2\rangle}\rvert$
f_0	$16.32 + 1.20i$ fm	16.36 fm	$1.73 + 0.13i$ fm	1.73 fm
σ	$0.43 + 0.31i$ fm	0.54 fm	$0.44 + 0.29i$ fm	0.53 fm
a_0	$0.56 - 1.25i$ fm	1.37 fm	$0.96 + 0.36i$ fm	1.02 fm

we can see that the results with the second method are much stable, and the ones with the first method have singularities when the cutoff moves the pole near the threshold where the binding energy becomes zero. As discussed in Ref. [84], the mean-squared radius is well defined with Eq. (24) both for the bound states and the resonances. Thus, at the end, we obtain $|\sqrt{\langle r^2\rangle}|_{f_0(980)} = 1.80 \pm 0.35$ fm, $|\sqrt{\langle r^2\rangle}|_{\sigma} = 0.68 \pm 0.05$ fm and $|\sqrt{\langle r^2\rangle}|_{a_0(980)} = 0.94 \pm 0.09$ fm, where we take the central value of the cutoff $q_{\max} = 931$ MeV within 15% uncertainties.

B. Single channel approach

In the previous section, we have investigated the properties of the σ, f_0, and a_0 states in the coupled channel

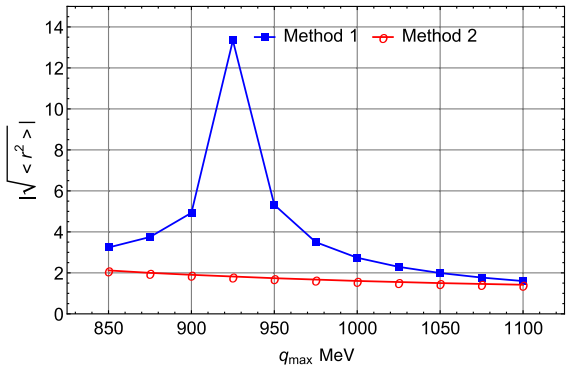

(a) The radii of $f_0(980)$.

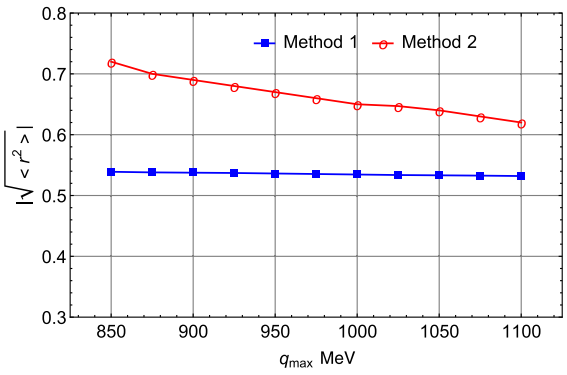

(b) The radii of σ.

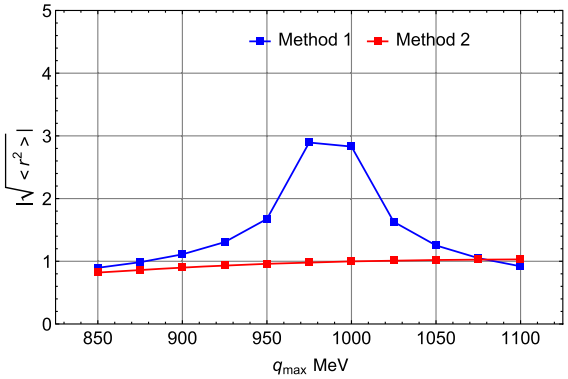

(c) The radii of $a_0(980)$.

FIG. 11. Results of the radii by varying the cutoffs, where method 1 means the radii calculated with Eq. (25), and method 2 the one with Eq. (24).

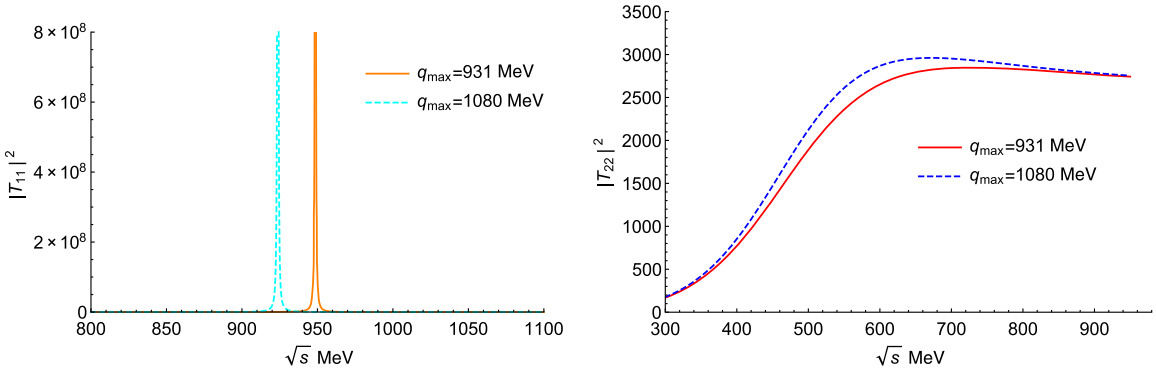

FIG. 12. Modulus squared of the $K\bar{K}$ (left) and $\pi\pi$ (right) scattering amplitudes.

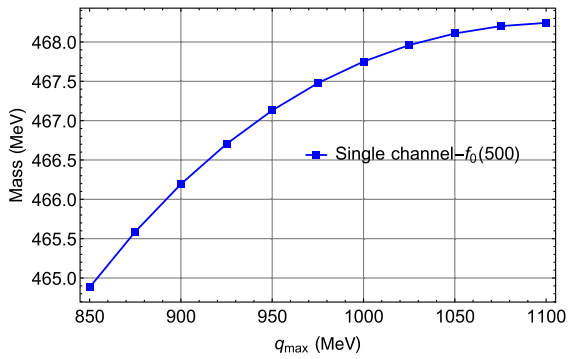

(a) Mass of the corresponding pole for σ state.

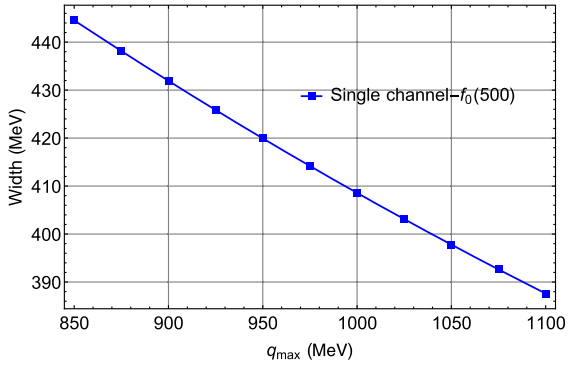

(b) Width of the corresponding pole for σ state.

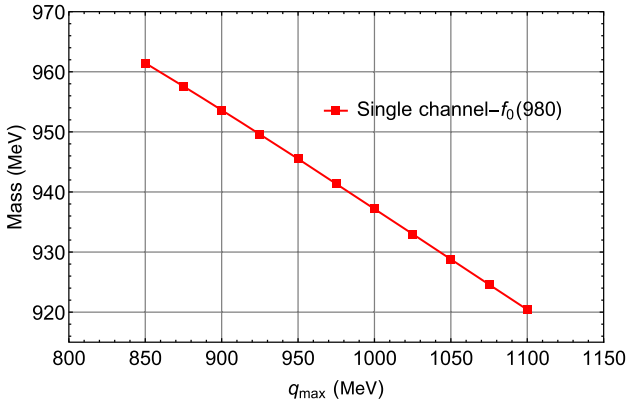

(c) Mass of the corresponding pole for $f_0(980)$ state.

FIG. 13. Results of the masses and widths for the states of σ and $f_0(980)$ as a function of the cutoffs.

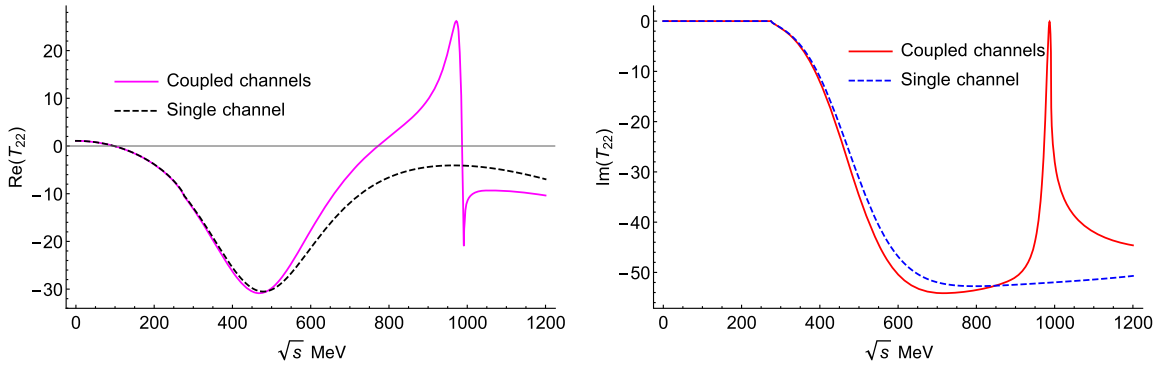

FIG. 14. Real (left) and imaginary (right) parts of the $\pi\pi$ scattering amplitude in coupled and single channels.

TABLE VII. Couplings of the σ and $f_0(980)$ states in a single channel.

$q_{\max} = 931$ MeV	$g_{K\bar{K}}g_{K\bar{K}}(\mathrm{GeV}^2)$	$\lvert g_{K\bar{K}}\rvert(\mathrm{GeV})$	$g_{\pi\pi}g_{\pi\pi}(\mathrm{GeV}^2)$	$\lvert g_{\pi\pi}\rvert(\mathrm{GeV})$
σ: $466.81 + 212.21i$	0	0	$-4.41 + 7.77i$	2.98
$f_0(980)$: 948.62	26.4	5.13	0	0
$q_{\max} = 1080$ MeV				
σ: $468.213 + 195.8i$	0	0	$-3.20 + 8.05i$	2.942
$f_0(980)$: 923.77	29.8	5.45	0	0

TABLE VIII. Compositeness of the σ and $f_0(980)$ states in single channel.

$q_{\max} = 931$ MeV	$(1-Z)_{K\bar{K}}$	$\lvert(1-Z)_{K\bar{K}}\rvert$	$(1-Z)_{\pi\pi}$	$\lvert(1-Z)_{\pi\pi}\rvert$
σ: $467.13 + 209.968i$	0	0	$-0.11 - 0.37i$	0.39
$f_0(980)$: 948.62	0.62	0.62	0	0
$q_{\max} = 1080$ MeV				
σ: $468.213 + 195.8i$	0	0	$-0.13 - 0.36i$	0.386
$f_0(980)$: 923.77	0.52	0.52	0	0

formalism. For the sake of the completeness and the comprehensive understanding of these dynamically generated states, we continue to examine their properties in single channel interactions where one can make a further checking their dominant components. At first, we show the results of the modulus squared of the scattering amplitudes, $|T|^2$, in Fig. 12, where one can see the sharp peak with nearly zero width in the $K\bar{K}$ channel on the left and the wide bump structure in the $\pi\pi$ channel on the right. Next, we search for the corresponding poles in the complex Riemann sheets. For the $\pi\pi$ channel interactions, as shown in Fig. 13 where we vary the cutoffs, we always find the pole in the second Riemann sheet above the threshold, of which the mass changes weakly and the width varies not so much as the case of the coupled channel interactions. For the case of the $K\bar{K}$ channel, now the pole keeps below the threshold, and thus, has no width as a pure bound state since there is no decay channel, see Fig. 13(c), which are more bound compared with the results of coupled channel cases in Fig. 8. Therefore, we can conclude that the σ state is a resonance mainly formed by the $\pi\pi$ interactions and the one of the f_0 state is a bound state of the $K\bar{K}$ component as found in the coupled channel interactions above. To reveal more details, see Fig. 14 for the real and the imaginary parts of the $\pi\pi$ scattering amplitudes in the coupled and the single channel interactions, one can see that in the region of the σ state appeared, 400–700 MeV, the amplitudes are not affected so much by the coupled channel of $K\bar{K}$, which is a bit far away from the threshold of $K\bar{K}$. Indeed, the structure of the $f_0(980)$ state can be clearly seen closed to the threshold of $K\bar{K}$, as shown in Fig. 14. However, in the isospin $I = 1$ sector, the potential of the $K\bar{K}$ channel is too weak to create a pole in the second Riemann sheet when it decouples to the $\pi\eta$ channel, of which the potential is independent with the energy. This means that the coupled channel effects play much important role in the dynamical production of the a_0 state.

As in case of the coupled channel interactions, we make further studies of the compositeness, the wave functions and the radii. The results of the couplings are given in

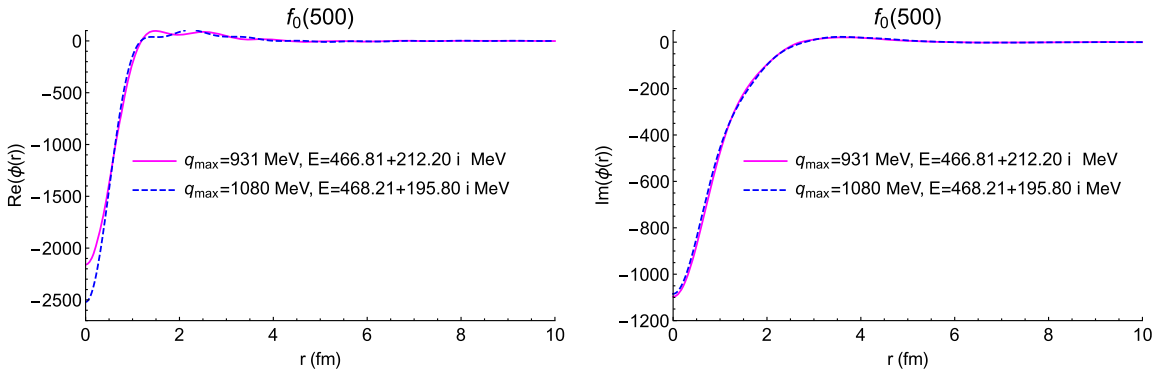

FIG. 15. Wave function of the σ state in the $\pi\pi$ channel.

TABLE IX. Radii of the states calculated with Eq. (24) in the single channel case.

Resonances	$q_{\max} = 931$ MeV	$\lvert\sqrt{\langle r^2\rangle}\rvert$	$q_{\max} = 1080$ MeV	$\lvert\sqrt{\langle r^2\rangle}\rvert$
σ	$0.69 + 0.007\,i$ fm	0.69 fm	$0.64 + 0.03\,i$ fm	0.64 fm
$f_0(980)$	1.29 fm	1.29 fm	1.11 fm	1.11 fm

TABLE X. Radii of the states evaluated with Eq. (25) in the single channel case.

Resonances	$q_{\max} = 931$ MeV	$\lvert\sqrt{\langle r^2\rangle}\rvert$	$q_{\max} = 1080$ MeV	$\lvert\sqrt{\langle r^2\rangle}\rvert$
σ	$0.43 + 0.32\,i$ fm	0.54 fm	$0.43 + 0.30\,i$ fm	0.53 fm
$f_0(980)$	0.75 fm	0.75 fm	0.55 fm	0.55 fm

Table VII, even though the strengths of the couplings have lost the relative meanings in the case of the single channel interactions. But, from the results of the compositeness, see Table VIII, with the couplings obtained, the compositeness for the $f_0(980)$ state is a bit smaller than the ones of the coupled channel case, which is consistent with the results of the coupled channel case in Table III.

The wave functions of the σ and $f_0(980)$ states are shown in Figs. 15 and 16, respectively. And their radii calculated from the form factor and the tail of the wave functions are given in Tables IX and X, respectively, of which the trajectories with different cutoffs are shown in Fig. 17. The results of Tables IX and X are consistent with the ones obtained in the coupled channel case, see Tables V and VI. Since now the $f_0(980)$ state is pure $K\bar{K}$ bound state, the radii with the tail of the wave functions in Eq. (25) are well defined and always smaller than the ones evaluated from the form factor with Eq. (24), compared the right part of Fig. 17 with the subfigure of Fig. 11(a).

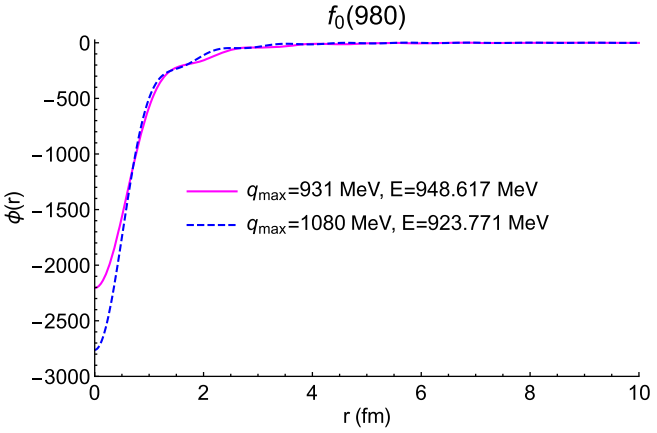

FIG. 16. Wave function of the $f_0(980)$ state in the $K\bar{K}$ channel.

IV. CONCLUSIONS

In the present work, we investigate the properties of the σ, $f_0(980)$, and $a_0(980)$ states with the chiral unitary approach, where we use the formalisms of the coupled channel and the single channel. Within the isospin limit, two poles are found in the second Riemann sheet in isospin $I = 0$ sector corresponding to the σ and $f_0(980)$ states, and a pole in $I = 1$ sector is found, which corresponds to the $a_0(980)$ state. In the case of the single channel calculations, we find the corresponding poles of the σ and $f_0(980)$ states in the $\pi\pi$ and $K\bar{K}$ channels with $I = 0$, respectively. However, in $I = 1$ sector the potential of the $K\bar{K}$ channel is too weak to create a pole in the second Riemann sheet.

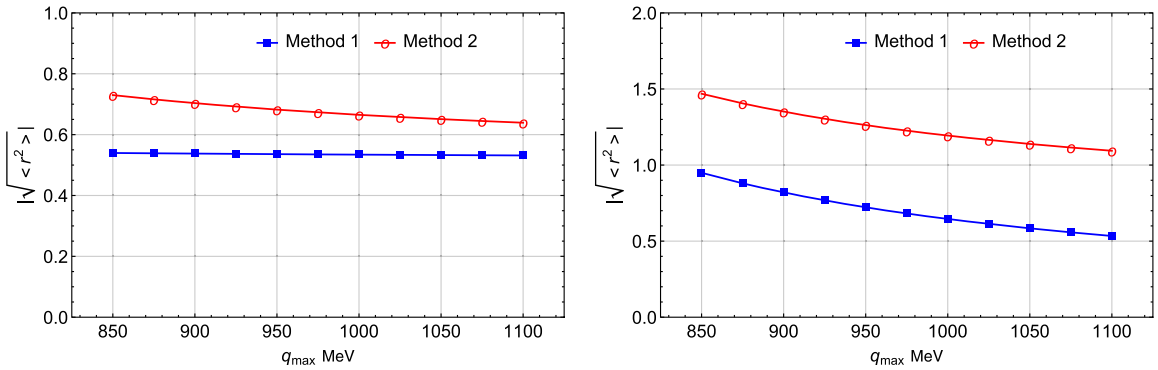

FIG. 17. Radii of the states σ (left) and $f_0(980)$ (right) as a function of cutoffs in single channel case, where the methods 1 and 2 are referred the same as in Fig. 11.

When we vary the only one free parameter of the cutoff, these states are stably dynamically generated both in the coupled channel and the single channel formalism, except for the one of $a_0(980)$ missing in the single channel interactions. Besides, we also predict the phase shifts in $I = 1$ sector with the coupled channel formalism.

Furthermore, we studied the couplings, the compositeness, the wave functions, and the mean-squared distance of these dynamically generated states in both the coupled channel and the single channel formalisms. From the results of the couplings and the compositeness, we conclude that the $f_0(980)$ state is essentially made by the $K\bar{K}$ component, which is about 80%, and has very small parts of $\pi\pi$. However, the σ state has the main contributions from the $\pi\pi$ channel, of which the component amounts to about 40%, and has quite small quantity of the $K\bar{K}$ component. Thus, the σ resonance has a large parts of something else except for the molecular components. For the case of the $a_0(980)$ state, the $\pi\eta$ channel has important contributions to its generations in the coupled channel interactions. Even though it is dominated by the $K\bar{K}$ component with 55%, it also has large contributions of about 16% from the $\pi\eta$ component. With the wave functions obtained, we calculate the radii of these states and get $|\sqrt{\langle r^2\rangle}|_{f_0(980)} = 1.80 \pm 0.35$ fm, $|\sqrt{\langle r^2\rangle}|_{\sigma} = 0.68 \pm 0.05$ fm and $|\sqrt{\langle r^2\rangle}|_{a_0(980)} = 0.94 \pm 0.09$ fm, which can be indirectly tested in the future experiments. Finally, from our results of the couplings, the compositeness, the wave functions and the radii, we can conclude that the $f_0(980)$ state is mainly a $K\bar{K}$ bound state, the σ state a resonance of $\pi\pi$ and the $a_0(980)$ state a loose $K\bar{K}$ bound state with the significant contributions from the $\pi\eta$ component.

ACKNOWLEDGMENTS

We thank Prof. B.-S. Zou for a careful reading of the manuscript and the useful comments, and Profs. C.-P. Shen, G.-F. Xu, Z.-H. Guo for the useful discussions. We also acknowledge Profs. N. N. Achasov, J. M. Frère and K. Azizi for the useful comments and the valuable informations.

[1] R. L. Jaffe, Phys. Rev. D **15**, 267 (1977).
[2] T. Cohen, F. J. Llanes-Estrada, J. R. Pelaez, and J. R. de Elvira, Phys. Rev. D **90**, 036003 (2014).
[3] J. M. Frère and J. Heeck, Phys. Rev. D **92**, 114035 (2015).
[4] H. X. Chen, W. Chen, X. Liu, and S. L. Zhu, Phys. Rep. **639**, 1 (2016).
[5] A. Hosaka, T. Iijima, K. Miyabayashi, Y. Sakai, and S. Yasui, Prog. Theor. Exp. Phys. (**2016**), 062C01.
[6] H. X. Chen, W. Chen, X. Liu, Y. R. Liu, and S. L. Zhu, Rep. Prog. Phys. **80**, 076201 (2017).
[7] R. F. Lebed, R. E. Mitchell, and E. S. Swanson, Prog. Part. Nucl. Phys. **93**, 143 (2017).
[8] A. Esposito, A. Pilloni, and A. D. Polosa, Phys. Rep. **668**, 1 (2017).
[9] F. K. Guo, C. Hanhart, U.-G. Meißner, Q. Wang, Q. Zhao, and B. S. Zou, Rev. Mod. Phys. **90**, 015004 (2018).
[10] A. Ali, J. S. Lange, and S. Stone, Prog. Part. Nucl. Phys. **97**, 123 (2017).
[11] S. L. Olsen, T. Skwarnicki, and D. Zieminska, Rev. Mod. Phys. **90**, 015003 (2018).
[12] M. Karliner, J. L. Rosner, and T. Skwarnicki, Annu. Rev. Nucl. Part. Sci. **68**, 17 (2018).
[13] C. Z. Yuan, Int. J. Mod. Phys. A **33**, 1830018 (2018).
[14] N. Brambilla, S. Eidelman, C. Hanhart, A. Nefediev, C. P. Shen, C. E. Thomas, A. Vairo, and C. Z. Yuan, arXiv: 1907.07583.
[15] J. B. Kogut, Rev. Mod. Phys. **55**, 775 (1983).
[16] M. Luscher, S. Sint, R. Sommer, and P. Weisz, Nucl. Phys. **B478**, 365 (1996).
[17] D. Mohler, S. Prelovsek, and R. M. Woloshyn, Phys. Rev. D **87**, 034501 (2013).
[18] M. A. Shifman, A. I. Vainshtein, and V. I. Zakharov, Nucl. Phys. **B147**, 385 (1979).
[19] L. J. Reinders, H. Rubinstein, and S. Yazaki, Phys. Rep. **127**, 1 (1985).
[20] J. M. Dias, R. M. Albuquerque, M. Nielsen, and C. M. Zanetti, Phys. Rev. D **86**, 116012 (2012).
[21] C. Hidalgo-Duque, J. Nieves, A. Ozpineci, and V. Zamiralov, Phys. Lett. B **727**, 432 (2013).
[22] S. S. Agaev, K. Azizi, and H. Sundu, Phys. Lett. B **781**, 279 (2018).
[23] S. S. Agaev, K. Azizi, and H. Sundu, Phys. Lett. B **784**, 266 (2018).
[24] S. S. Agaev, K. Azizi, and H. Sundu, Phys. Lett. B **789**, 405 (2019).
[25] H. D. Politzer and M. B. Wise, Phys. Lett. B **208**, 504 (1988).
[26] H. Georgi, Phys. Lett. B **240**, 447 (1990).
[27] E. Epelbaum, H. W. Hammer, and U.-G. Meißner, Rev. Mod. Phys. **81**, 1773 (2009).
[28] N. Kaiser, P. B. Siegel, and W. Weise, Phys. Lett. B **362**, 23 (1995).
[29] J. A. Oller, E. Oset, and A. Ramos, Prog. Part. Nucl. Phys. **45**, 157 (2000).
[30] J. A. Oller and U.-G. Meißner, Phys. Lett. B **500**, 263 (2001).
[31] T. Hyodo, D. Jido, and A. Hosaka, Phys. Rev. C **78**, 025203 (2008).
[32] E. Oset, L. S. Geng, D. Gamermann, M. J. Vicente Vacas, D. Strottman, K. P. Khemchandani, A. Martinez Torres, J. A. Oller, L. Roca, and M. Napsuciale, Int. J. Mod. Phys. E **18**, 1389 (2009).

[33] F. Giacosa, Phys. Rev. D **80**, 074028 (2009).
[34] C. W. Xiao, U.-G. Meißner, and J. A. Oller, Eur. Phys. J. A **56**, 23 (2020).
[35] S. D. Protopopescu, M. Alston-Garnjost, A. Barbaro-Galtieri, S. M. Flatté, J. H. Friedman, T. A. Lasinski, G. R. Lynch, M. S. Rabin, and F. T. Solmitz, Phys. Rev. D 1973) 1279 ,**7**).
[36] R. Ammar, R. Davis, W. Kropac, J. Mott, D. Slate, B. Werner, M. Derrick, T. Fields, and F. Schweingruber, Phys. Rev. Lett. **21**, 1832 (1968).
[37] D. Morgan, Phys. Lett. **51B**, 71 (1974).
[38] D. Morgan and M. R. Pennington, Z. Phys. C **48**, 623 (1990).
[39] D. Morgan and M. R. Pennington, Phys. Rev. D **48**, 1185 (1993).
[40] N. A. Tornqvist and M. Roos, Phys. Rev. Lett. **76**, 1575 (1996).
[41] R. L. Jaffe, Phys. Rev. D **15**, 281 (1977).
[42] N. N. Achasov, Nucl. Phys. **A728**, 425 (2003).
[43] J. D. Weinstein and N. Isgur, Phys. Rev. Lett. **48**, 659 (1982).
[44] J. D. Weinstein and N. Isgur, Phys. Rev. D **27**, 588 (1983).
[45] J. D. Weinstein and N. Isgur, Phys. Rev. D **41**, 2236 (1990).
[46] G. Janssen, B. C. Pearce, K. Holinde, and J. Speth, Phys. Rev. D **52**, 2690 (1995).
[47] N. N. Achasov and G. N. Shestakov, Phys. Usp. **54**, 799 (2011).
[48] N. N. Achasov, Phys. Part. Nucl. **48**, 681 (2017).
[49] N. N. Achasov and G. N. Shestakov, Phys. Usp. **62**, 3 (2019).
[50] J. R. Pelaez, Phys. Rep. **658**, 1 (2016).
[51] J. R. Pelaez, Mod. Phys. Lett. A **19**, 2879 (2004).
[52] J. R. Pelaez, Phys. Rev. Lett. **92**, 102001 (2004).
[53] K. Nakamura *et al.* (Particle Data Group), J. Phys. G **37**, 075021 (2010).
[54] Z. H. Guo and J. A. Oller, Phys. Rev. D **84**, 034005 (2011).
[55] Z. H. Guo, J. A. Oller, and J. Ruiz de Elvira, Phys. Rev. D **86**, 054006 (2012).
[56] J. A. Oller and E. Oset, Nucl. Phys. **A620**, 438 (1997); **A652**, 407(E) (1999).
[57] J. Gasser and H. Leutwyler, Nucl. Phys. **B250**, 465 (1985).
[58] U.-G. Meißner, Rep. Prog. Phys. **56**, 903 (1993).
[59] A. Pich, Rep. Prog. Phys. **58**, 563 (1995).
[60] G. Ecker, Prog. Part. Nucl. Phys. **35**, 1 (1995).
[61] V. Bernard, N. Kaiser, and U.-G. Meißner, Int. J. Mod. Phys. E **04**, 193 (1995).
[62] S. Scherer, Adv. Nucl. Phys. **27**, 277 (2003).
[63] M. Tanabashi *et al.* (Particle Data Group), Phys. Rev. D **98**, 030001 (2018).
[64] J. A. Oller, E. Oset, and J. R. Pelaez, Phys. Rev. D **59**, 074001 (1999); **60**, 099906(E) (1999); **75**, 099903(E) (2007).
[65] J. A. Oller and U.-G. Meißner, Phys. Lett. B **500**, 263 (2001).
[66] F. K. Guo, P. N. Shen, H. C. Chiang, R. G. Ping, and B. S. Zou, Phys. Lett. B **641**, 278 (2006).
[67] J. A. Oller, Phys. Rev. D **71**, 054030 (2005).
[68] A. Ozpineci, C. W. Xiao, and E. Oset, Phys. Rev. D **88**, 034018 (2013).
[69] J. A. Oller and E. Oset, Phys. Rev. D **60**, 074023 (1999).
[70] S. Weinberg, Phys. Rev. **137**, B672 (1965).
[71] F. Aceti and E. Oset, Phys. Rev. D **86**, 014012 (2012).
[72] T. Hyodo, D. Jido, and A. Hosaka, Phys. Rev. C **85**, 015201 (2012).
[73] T. Sekihara and T. Hyodo, Phys. Rev. C **87**, 045202 (2013).
[74] C. W. Xiao, F. Aceti, and M. Bayar, Eur. Phys. J. A **49**, 22 (2013).
[75] T. Hyodo, Phys. Rev. Lett. **111**, 132002 (2013).
[76] F. Aceti, L. R. Dai, L. S. Geng, E. Oset, and Y. Zhang, Eur. Phys. J. A **50**, 57 (2014).
[77] Z. H. Guo and J. A. Oller, Phys. Rev. D **93**, 096001 (2016).
[78] J. Yamagata-Sekihara, J. Nieves, and E. Oset, Phys. Rev. D **83**, 014003 (2011).
[79] D. Gamermann, J. Nieves, E. Oset, and E. Ruiz Arriola, Phys. Rev. D **81**, 014029 (2010).
[80] T. Sekihara, T. Hyodo, and D. Jido, Prog. Theor. Exp. Phys. (**2015**), 63D04.
[81] J. Vijande and A. Valcarce, Phys. Rev. C **80**, 035204 (2009).
[82] A. Valcarce and J. Vijande, Chin. Phys. C **34**, 1290 (2010).
[83] J. Vijande and A. Valcarce, Symmetry **1**, 155 (2009).
[84] T. Sekihara, T. Hyodo, and D. Jido, Phys. Rev. C **83**, 055202 (2011).
[85] L. Y. Dai, X. W. Kang, T. Luo, and U.-G. Meißner, Commun. Theor. Phys. **71**, 1309 (2019).
[86] S. M. Flatte, Phys. Lett. **63B**, 224 (1976).
[87] F. K. Guo, X. H. Liu, and S. Sakai, Prog. Part. Nucl. Phys. **112**, 103757 (2020).
[88] V. Baru, J. Haidenbauer, C. Hanhart, Y. Kalashnikova, and A. E. Kudryavtsev, Phys. Lett. B **586**, 53 (2004).